

# A new analysis of transverse momentum spectra of various jets produced in high energy collisions

Yang-Ming Tai<sup>1,2,\*</sup>, Pei-Pin Yang<sup>1,2,†</sup>, Fu-Hu Liu<sup>1,2,‡</sup>

<sup>1</sup>*Institute of Theoretical Physics & State Key Laboratory of Quantum Optics and Quantum Optics Devices,*

*Shanxi University, Taiyuan, Shanxi 030006, People's Republic of China*

<sup>2</sup>*Collaborative Innovation Center of Extreme Optics, Shanxi University,*

*Taiyuan, Shanxi 030006, People's Republic of China*

**Abstract:** With the framework of the multi-source thermal model, we analyze the experimental transverse momentum spectra of various jets produced in different collisions at high energies. A projectile participant quark and a target participant quark are considered. Each participant quark is assumed to contribute to the transverse momentum distribution to be the TP-like function, i.e. a revised Tsallis–Pareto-type function. The contribution of the two participant quarks to the transverse momentum distribution is then the convolution of two TP-like functions. The model distribution can be used to fit the experimental spectra measured by different collaborations. The related parameters such as the entropy index-related, effective temperature, and revised index are then obtained. The trends of these parameters are useful to understand the characteristic of high energy collisions.

**Keywords:** Transverse momentum spectra, High-energy jets, TP-like function

**PACS:** 12.40.Ee, 13.87.Fh, 25.75.Ag, 24.10.Pa

## 1 Introduction

In central heavy ion (nucleus-nucleus) collisions at high energy, quark-gluon plasma (QGP) is believed to create possibly [1, 2, 3], because the environment of high temperature and density is formed. After the formation, QGP experiences the process of hadronization and then produces lots of final-state particles. Meanwhile, at the early stage of collisions, some products such as various jets are produced and interact subsequently with QGP. Because of the interactions between jets and QGP, jets lost their energies when they go through QGP region. Not only lots of identified particles but also various jets can be measured in experiments at high energies. Indeed, in the abundant data on high energy collisions, the data on various jets are one of the most important constituents. We are interested in analyzing the experimental transverse momentum ( $p_T$ ) spectra of various jets, because they can reflect some information of early collisions of participant quarks or partons.

Generally, the  $p_T$  spectra of various jets are wider

than those of identified particles. In fact, both the  $p_T$  spectra of various jets and identified particles cover a wide  $p_T$  range. Even if for the later, one may divide the  $p_T$  range into low- and high- $p_T$  regions. It is expected that the spectra in low- $p_T$  region are contributed by the soft excitation process, while the spectra in high- $p_T$  region are contributed by the hard scattering process. In some cases, the spectra in low- and high- $p_T$  regions are still complex. One may divide further the low- and high- $p_T$  regions into very low- and low- $p_T$  regions as well as high- and very high- $p_T$  regions respectively. It is expected that the spectra in different  $p_T$  regions can be analyzed by different functions. This means that one needs two-component or even four-component function to fit the wide  $p_T$  spectra.

As an example, we discuss the two-component function. There are two methods to superpose the two components in a function [4, 5, 6]. The first method uses a weighted sum for the two components and there are correlations between the parameters of the two compo-

\*E-mail: tayangming6@qq.com

†E-mail: yangpeipin@qq.com; peipinyangshanxi@163.com

‡Corresponding author. E-mail: fuhuliu@163.com; fuhuliu@sxu.edu.cn

nents, though the point of linkage is smooth. The second method uses a step function to link the two components [6] and there is a non-smooth linkage between the two components, though the parameters are uncorrelative. It is imaginable that more issues will appear if we consider four components in a function. Although the two-component function is widely used in literature, it is not an ideal treatment method, not to mention the four-component function. We hope to use a new method to treat the two or four components uniformly. Even a single component function is used to fit the spectra in wide  $p_T$  range.

Fortunately, to search for the single component function for the spectra in wide  $p_T$  range is possible, because the similarity, universality, or common law is existent in high energy collisions [7, 8, 9, 10, 11, 12, 13]. To search for the single component function, we have tested many potential functions. Finally, we have found that the convolution of two or more revised Tsallis–Pareto-type functions [14, 15] is a suitable choice. For the purpose of doing a convenient description, we call the revised Tsallis–Pareto-type function the TP-like function in our recent work [15] and this paper. The application of the convolution of two or more functions is a general treatment method with the framework of the multi-source thermal model [5], where the considered distributions are assumed from the contributions of two or more sources. The considered distributions include at least the multiplicity, transverse energy, and transverse momentum (transverse mass) distributions.

In this paper, in the framework of the multi-source thermal model, we assume that a projectile participant quark and a target participant quark take part in the production of various jets, and they contribute to the  $p_T$  distribution to be the TP-like function [14, 15]. Then, we may use the convolution of two TP-like functions to fit the experimental  $p_T$  spectra of various jets. The related data quoted in this paper are from proton-(anti)proton (p-p(̄p)), deuteron-gold (d-Au), gold-gold (Au-Au), proton-lead (p-Pb), and lead-lead (Pb-Pb) collisions, with different selection conditions, over a center-of-mass energy ( $\sqrt{s_{NN}}$ , or simplified as  $\sqrt{s}$  for p-p(̄p) collisions) range from 0.2 to 13 TeV.

The remainder of this paper is structured in the following. The formalism and method are described in Section 2. The results and discussion are given in Section 3. Finally, we give the summary and conclusions in

Section 4.

## 2 The formalism and method

According to ref. [14], the Tsallis–Pareto-type function which describes empirically the  $p_T$  spectra of particles with rest mass  $m_0$  can be given by

$$f_{p_T}(p_T) = C p_T \left( 1 + \frac{\sqrt{p_T^2 + m_0^2} - m_0}{nT} \right)^{-n} \quad (1)$$

which is a probability density function and  $C$  is the normalization constant because  $\int_0^\infty f_{p_T}(p_T) dp_T = 1$ . In Eq. (1), as an entropy index-related parameter,  $n$  is related to the entropy index  $q$  because  $n = 1/(q - 1)$ . Generally,  $q = 1$  or  $n = \infty$  means an equilibrium state. If  $q$  is close to 1 or  $n$  is large enough, the system is close to an equilibrium state. The free parameter  $T$  in Eq. (1) is an effective temperature that describes the excitation and expansion degree of the emission source for particles. We call  $T$  the effective temperature because both the contributions of random thermal motion and flow effect are included.

Equation (1) is not flexible enough in the description of  $p_T$  spectra of particles, in particular for the spectra in low- $p_T$  region. Empirically, Eq. (1) can be revised artificially by adding a revised index  $a_0$  that is non-dimensional as the power index of  $p_T$ . Then, we have the TP-like function to be [15]

$$f_{p_T}(p_T) = C p_T^{a_0} \left( 1 + \frac{\sqrt{p_T^2 + m_0^2} - m_0}{nT} \right)^{-n}, \quad (2)$$

where  $C$  is the normalization constant which is different from that in Eq. (1). For the purpose of convenience, two normalization constants in Eqs. (1) and (2) are represented by the same symbol  $C$ , though they may be different. Although one more parameter is introduced, Eq. (2) is more accurate than Eq. (1). In particular, we can obtain Eq. (1) from Eq. (2) if we use  $a_0 = 1$ .

With the framework of the multi-source thermal model [5], we assume that many quarks or partons take part in the collisions. For a given particle or jet, two quarks, i.e. a projectile participant (the first) quark and a target participant (the second) quark, play main role in the production process. The contribution amount or portion ( $p_{ti}$ ) of each quark to  $p_T$  is assumed to obey the TP-like function, where  $i = 1$  and 2 are for the first and second quarks respectively. The TP-like function

obeyed by  $p_{ti}$  is [15]

$$f_i(p_{ti}) = C_i p_{ti}^{a_0} \left( 1 + \frac{\sqrt{p_{ti}^2 + m_{0i}^2} - m_{0i}}{nT} \right)^{-n}, \quad (3)$$

where  $m_{0i}$  is empirically the constituent mass of the  $i$ -th participant quark.

The total amount contributed by the two quarks is the convolution of two TP-like functions. That is [15]

$$f_{p_T}(p_T) = \int_0^{p_T} f_1(p_{t1}) f_2(p_T - p_{t1}) dp_{t1} \quad (4)$$

or

$$f_{p_T}(p_T) = \int_0^{p_T} f_2(p_{t2}) f_1(p_T - p_{t2}) dp_{t2}. \quad (5)$$

In most cases, the convolution of two TP-like functions is suitable for the spectra of various jets. Correspondingly, two heavy flavor quarks such as  $c + \bar{c}$ ,  $b + \bar{b}$ , or  $t + \bar{t}$  should be considered due to more effective energy being needed. For two light flavor quarks such as  $u + \bar{u}$ ,  $d + \bar{d}$ , or  $s + \bar{s}$ , we do not need to consider them due to too less effective energy for the production of various jets.

The method of the convolution of three TP-like functions is similar to that of two TP-like functions. Firstly, we may obtain the convolution  $f_{12}(p_{t12})$  of the first two TP-like functions  $f_1(p_{t1})$  and  $f_2(p_{t2})$ . Secondly, we may obtain the convolution  $f_{p_T}(p_T)$  of  $f_{12}(p_{t12})$  and  $f_3(p_{t3})$ . Alternatively, we may obtain firstly the convolution  $f_{23}(p_{t23})$  of the last two TP-like functions  $f_2(p_{t2})$  and  $f_3(p_{t3})$ , and then we may obtain the convolution  $f_{p_T}(p_T)$  of  $f_1(p_{t1})$  and  $f_{23}(p_{t23})$ . The same idea can be used for the convolution of more than three TP-like functions. At present, the convolution of a projectile participant quark and a target participant quark is enough to fit the spectra of  $p_T$  of various jets. Temporarily, we do not need to consider the convolution of three or more participant quarks.

Because of the introduction of  $a_0$ , Eq. (2) is more accurate and flexible than Eq. (1). By using  $a_0$ , the spectra in very low- $p_T$  region can be described reasonable. With the framework of the multi-source thermal model, the method of the convolution of two or more probability density functions is applicable for not only the spectra of  $p_T$  but also the spectra of multiplicity and transverse energy. In the method, to search for the probability density function contributed by a single participant or contributor or source is a key issue. This participant or contributor or source can be quark if we

study the spectra of particles, or nucleon if we study the spectra of nuclear fragments.

### 3 Results and discussion

Figure 1 shows the transverse momentum  $p_T$  spectra of different jets produced in (a) p-p, (b) d-Au, and (c) Au-Au collisions with mid-pseudorapidity (mid- $\eta$ ,  $|\eta| < 0.5$  for Figs. 1(a) and 1(c) and  $|\eta| < 0.55$  for Fig. 1(b)), as well as in (d) p-p collisions with non-mid- $\eta$  ( $0.8 < \eta < 1.8$ ) at  $\sqrt{s_{NN}} = 0.2$  TeV, where  $N$  and  $N_{\text{evt}}$  denote the numbers of jets and events respectively. The symbols are cited from the experimental data measured by the STAR Collaboration [16, 17, 18]. In Figs. 1(a) and 1(c), the high tower (HT) trigger jets were selected. In Fig. 1(a)–(c), the jet events were selected using a cone radius ( $R = 0.4$ ) and anti- $k_T$  algorithm [19], where  $k_T$  denotes the transverse momentum. In Figs. 1(b) and 1(c), the data of d-Au and Au-Au collisions were measured in 0–20% centrality class. In the figure, the curves are our fitted results with Eq. (4). In the fit process, two participant top quarks with constituent mass of 174  $\text{GeV}/c^2$  for each one are considered. The values of free parameters ( $n$ ,  $T$ , and  $a_0$ ), normalization constant ( $N_0$ ),  $\chi^2$ , and number of degree of freedom (ndof) are listed in Table 1. One can see that the  $p_T$  spectra of different jets are shown to obey approximately the convolution of two TP-like functions. The values of mean excitation and expansion degree (defined by the effective temperature parameter  $T$ ) seem to not related to the size of collision system in the error range.

Figure 2(a) presents the  $p_T$  spectra of fast jets produced in p-Pb collisions with different centralities at  $\sqrt{s_{NN}} = 5.02$  TeV, where  $\sigma$  on the vertical axis denotes the cross section. The  $p_T$  spectra of charged jets produced in Pb-Pb collisions with different centralities at  $\sqrt{s_{NN}} = 2.76$  TeV are presented in Fig. 2(b), where  $N_{\text{coll}}$  on the vertical axis denotes the number of binary nucleon-nucleon collisions. The symbols are cited from the experimental data measured by the ALICE Collaboration [20, 21]. The jet events were selected with a cone radius ( $R = 0.2$ ) and mid- $\eta$  ( $|\eta| < 0.5$ ). The curves are our fitted results with Eq. (4), in which two participant top quarks are considered. The values of  $n$ ,  $T$ ,  $a_0$ ,  $N_0$ ,  $\chi^2$ , and ndof are listed in Table 1. One can see that the convolution of two TP-like functions describes approximately the experimental data of the mentioned

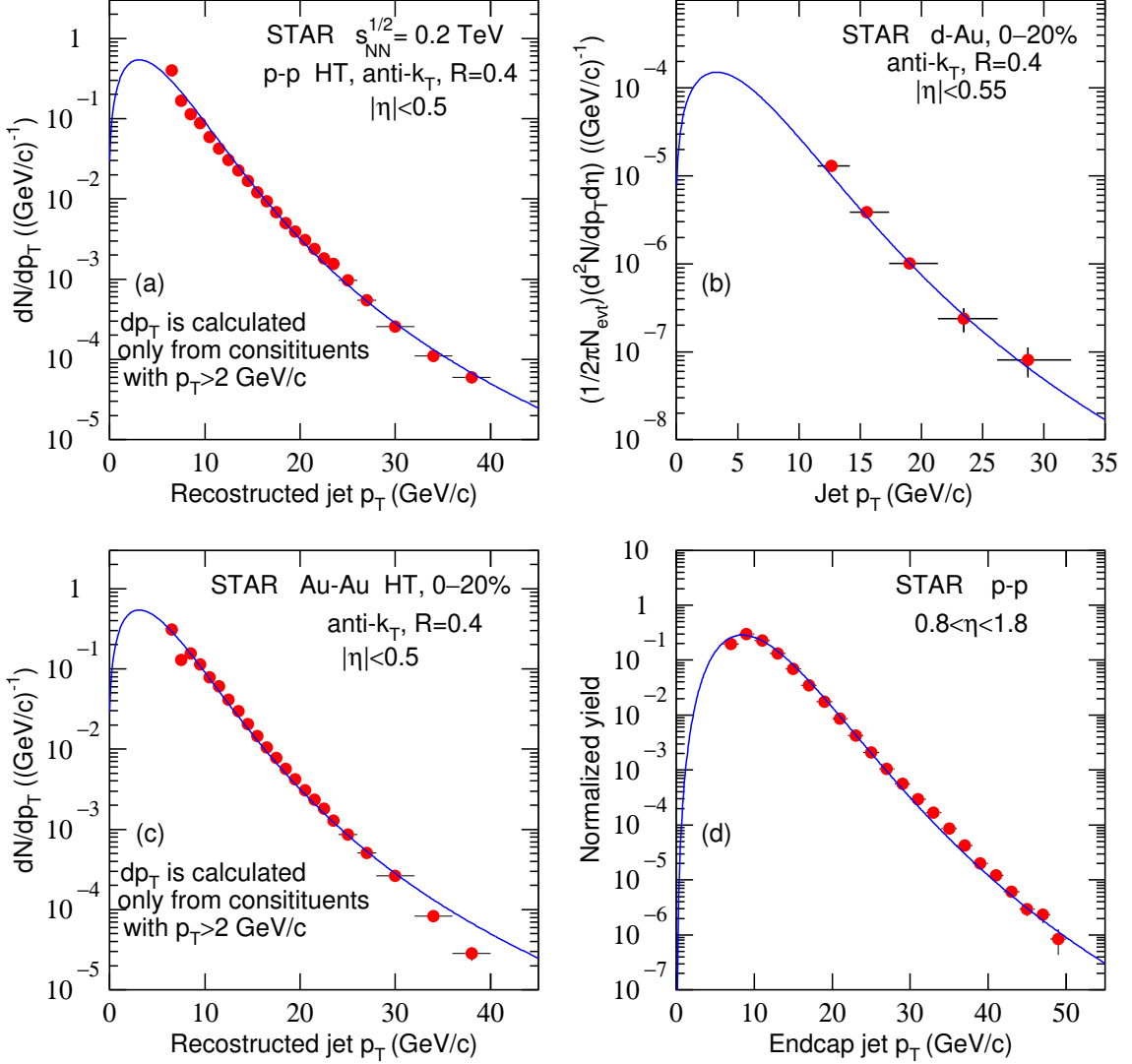


Fig. 1. Transverse momentum spectra of different jets produced in (a) p-p, (b) d-Au, and (c) Au-Au collisions with mid- $\eta$  ( $|\eta| < 0.5$  or  $0.55$ ), as well as in (d) p-p collisions with non-mid- $\eta$  ( $0.8 < \eta < 1.8$ ) at  $\sqrt{s_{NN}} = 0.2$  TeV. The symbols are cited from the experimental data measured by the STAR Collaboration [16, 17, 18] and the curves are our fitted results with Eq. (4).

jets. The effective temperature parameter  $T$  are the same with changing the centrality percentage in p-Pb collisions. And in Pb-Pb collisions,  $T$  increases slightly with the increase of centrality percentage, i.e.  $T$  decreases slightly with the increase of centrality itself.

Figure 3(a) (3(b)) presents the  $p_T$  spectrum of leading jets corresponding to the  $Z \rightarrow \mu\mu$  ( $Z \rightarrow ee$ ) channel in p- $\bar{p}$  collisions at  $\sqrt{s} = 1.96$  TeV. Figure 3(c) (3(d)) presents the  $p_T$  spectra of jets ( $b$ -jets) corresponding to the lepton and dilepton channels in p-p collisions at  $\sqrt{s} = 7$  TeV. The symbols are cited from the experimental data measured by the D0 [22, 23], CMS [24],

and ATLAS Collaborations [25]. In Figs. 3(a) and 3(b), the jet events were selected with a cone radius ( $R = 0.5$ ) and wide  $\eta$  range ( $|\eta| < 2.5$ ). In Fig. 3(c) and 3(d), the jet events were selected with  $|\eta| < 2.4$  and  $|\eta| < 2.5$  respectively. The curves are our fitted results with Eq. (4), in which two participant top quarks are considered for Figs. 3(a)–3(c), and two participant bottom quarks with constituent mass of  $4.19$  GeV/ $c^2$  for each one are considered for Fig. 3(d). The values of  $n$ ,  $T$ ,  $a_0$ ,  $N_0$ ,  $\chi^2$ , and ndof are listed in Table 1. One can see that the convolution of two TP-like functions provides an approximate description on the data. The effective temperature

Table 1. Values of  $n$ ,  $T$ ,  $a_0$ ,  $N_0$  ( $\sigma_0$ ),  $\chi^2$ , and ndof corresponding to the curves in Figs. 1–9, where  $\sigma_0$  is only for Fig. 2(a).

Figure	Collision	$n$	$T$ (GeV)	$a_0$	$N_0$ [ $\sigma_0$ (mb)]	$\chi^2/\text{ndof}$
1(a), p-p, $ \eta  < 0.5$	$t + \bar{t}$	$2.80 \pm 0.12$	$0.032 \pm 0.008$	$0.00 \pm 0.01$	$3.499 \pm 0.002$	225/19
1(b), d-Au, $ \eta  < 0.55$	$t + \bar{t}$	$3.40 \pm 0.02$	$0.036 \pm 0.008$	$0.00 \pm 0.01$	$0.007 \pm 0.001$	5/1
1(c), Au-Au, $ \eta  < 0.5$	$t + \bar{t}$	$3.20 \pm 0.05$	$0.040 \pm 0.009$	$0.00 \pm 0.05$	$2.999 \pm 0.002$	249/19
1(d), p-p, $0.8 < \eta < 1.8$	$t + \bar{t}$	$6.00 \pm 0.05$	$0.045 \pm 0.001$	$1.50 \pm 0.01$	$2.499 \pm 0.002$	195/18
2(a), p-Pb, 0–20%	$t + \bar{t}$	$3.00 \pm 0.01$	$0.130 \pm 0.002$	$1.00 \pm 0.02$	$0.999 \pm 0.001$	18/4
2(a), p-Pb, 20–40%	$t + \bar{t}$	$3.00 \pm 0.02$	$0.130 \pm 0.001$	$1.00 \pm 0.02$	$0.699 \pm 0.002$	11/3
2(a), p-Pb, 40–60%	$t + \bar{t}$	$3.00 \pm 0.01$	$0.130 \pm 0.003$	$1.00 \pm 0.02$	$0.499 \pm 0.001$	12/2
2(a), p-Pb, 60–80%	$t + \bar{t}$	$3.00 \pm 0.03$	$0.130 \pm 0.001$	$1.00 \pm 0.02$	$0.299 \pm 0.002$	18/2
2(a), p-Pb, 80–100%	$t + \bar{t}$	$3.00 \pm 0.05$	$0.130 \pm 0.001$	$1.00 \pm 0.02$	$0.149 \pm 0.002$	6/1
2(b), Pb-Pb, 0–10%	$t + \bar{t}$	$3.00 \pm 0.11$	$0.130 \pm 0.050$	$1.00 \pm 0.01$	$(1.799 \pm 0.001) \times 10^{-5}$	8/5
2(b), Pb-Pb, 10–30%	$t + \bar{t}$	$3.00 \pm 0.05$	$0.140 \pm 0.051$	$1.00 \pm 0.01$	$(2.299 \pm 0.001) \times 10^{-5}$	3/5
2(b), Pb-Pb, 30–50%	$t + \bar{t}$	$3.00 \pm 0.21$	$0.150 \pm 0.052$	$1.00 \pm 0.01$	$(2.999 \pm 0.001) \times 10^{-5}$	4/4
2(b), Pb-Pb, 50–80%	$t + \bar{t}$	$3.00 \pm 0.31$	$0.150 \pm 0.051$	$1.00 \pm 0.01$	$(3.999 \pm 0.002) \times 10^{-5}$	7/3
3(a), p- $\bar{p}$ , $Z \rightarrow \mu\mu$	$t + \bar{t}$	$2.10 \pm 0.02$	$1.150 \pm 0.091$	$-0.45 \pm 0.01$	$259969.508 \pm 2.200$	106/31
3(b), p- $\bar{p}$ , $Z \rightarrow ee$	$t + \bar{t}$	$2.05 \pm 0.05$	$1.200 \pm 0.092$	$-0.45 \pm 0.01$	$239964.205 \pm 2.522$	104/31
3(c), p-p, lepton+jet	$t + \bar{t}$	$5.00 \pm 0.55$	$13.000 \pm 0.853$	$-0.48 \pm 0.01$	$199762.511 \pm 11.050$	257/18
3(c), p-p, dilepton+jet	$t + \bar{t}$	$5.00 \pm 0.80$	$12.000 \pm 0.852$	$-0.48 \pm 0.01$	$51954.412 \pm 2.502$	201/19
3(d), p-p, lepton+b-jet	$b + \bar{b}$	$10.00 \pm 1.50$	$12.000 \pm 0.893$	$1.00 \pm 0.01$	$19997.136 \pm 0.520$	133/29
3(d), p-p, dilepton+b-jet	$b + \bar{b}$	$10.00 \pm 1.50$	$12.000 \pm 0.955$	$1.00 \pm 0.01$	$2599.627 \pm 0.223$	57/25
4(a), 7 TeV p-p, $e+b$ -jet	$b + \bar{b}$	$16.00 \pm 0.03$	$15.000 \pm 1.512$	$1.00 \pm 0.03$	$13999.407 \pm 0.620$	345/12
4(b), 7 TeV p-p, $\mu+b$ -jet	$b + \bar{b}$	$16.00 \pm 0.05$	$16.000 \pm 1.502$	$1.00 \pm 0.01$	$14998.827 \pm 0.953$	230/12
4(c), 7 TeV p-p, $e$ +jet	$t + \bar{t}$	$3.40 \pm 0.15$	$3.500 \pm 0.550$	$1.60 \pm 0.13$	$27400.066 \pm 0.965$	859/20
4(d), 7 TeV p-p, $\mu$ +jet	$t + \bar{t}$	$3.50 \pm 0.12$	$3.500 \pm 0.521$	$1.50 \pm 0.10$	$34924.095 \pm 0.856$	155/20
4(e), 8 TeV p-p, $e$ +jet	$t + \bar{t}$	$3.50 \pm 0.42$	$3.000 \pm 0.552$	$1.50 \pm 0.01$	$119830.499 \pm 2.505$	509/16
4(f), 8 TeV p-p, $\mu$ +jet	$t + \bar{t}$	$3.20 \pm 0.35$	$3.000 \pm 0.512$	$1.40 \pm 0.05$	$159633.552 \pm 3.254$	832/15
5, leading jet	$t + \bar{t}$	$3.00 \pm 0.02$	$3.600 \pm 0.195$	$1.10 \pm 0.12$	$43983.362 \pm 2.562$	19/4
5, 2 <sup>nd</sup> jet	$t + \bar{t}$	$3.00 \pm 0.02$	$1.000 \pm 0.190$	$1.70 \pm 0.15$	$41991.806 \pm 3.255$	20/3
5, 3 <sup>rd</sup> jet	$t + \bar{t}$	$2.50 \pm 0.01$	$0.600 \pm 0.185$	$1.00 \pm 0.14$	$42998.320 \pm 3.235$	6/2
5, 4 <sup>th</sup> jet	$t + \bar{t}$	$2.50 \pm 0.01$	$0.300 \pm 0.095$	$1.00 \pm 0.16$	$29999.717 \pm 2.253$	8/1
5, 5 <sup>th</sup> jet	$t + \bar{t}$	$2.50 \pm 0.01$	$0.150 \pm 0.090$	$1.00 \pm 0.12$	$24999.942 \pm 1.025$	7/0
6(a), leading $b$ -jet	$b + \bar{b}$	$9.00 \pm 0.06$	$13.000 \pm 1.506$	$1.00 \pm 0.05$	$1097.905 \pm 0.252$	98/20
6(b), subleading $b$ -jet	$b + \bar{b}$	$6.00 \pm 0.10$	$4.800 \pm 0.502$	$1.00 \pm 0.03$	$1498.243 \pm 0.586$	11/10
6(c), leading jet	$t + \bar{t}$	$2.01 \pm 0.15$	$7.000 \pm 0.520$	$-0.48 \pm 0.01$	$4998.740 \pm 1.562$	94/14
6(d), subleading jet	$t + \bar{t}$	$2.10 \pm 0.22$	$2.050 \pm 0.510$	$-0.48 \pm 0.01$	$6965.727 \pm 0.852$	37/14
7(a), leading light jet	$c + \bar{c}$	$5.00 \pm 0.18$	$11.000 \pm 1.505$	$1.00 \pm 0.02$	$5629.301 \pm 0.560$	147/36
7(b), subleading light jet	$c + \bar{c}$	$5.50 \pm 0.12$	$4.500 \pm 0.150$	$1.00 \pm 0.01$	$11848.861 \pm 0.805$	89/36
7(c), leading jet	$t + \bar{t}$	$2.50 \pm 0.15$	$5.000 \pm 0.502$	$0.00 \pm 0.03$	$399824.415 \pm 5.600$	16/32
7(d), subleading jet	$t + \bar{t}$	$2.50 \pm 0.17$	$2.000 \pm 0.105$	$0.00 \pm 0.01$	$499979.349 \pm 2.354$	28/32
8(a), small-R $e$ +jet	$t + \bar{t}$	$70.00 \pm 10.10$	$70.000 \pm 15.100$	$-0.50 \pm 0.02$	$39936.022 \pm 0.500$	23/16
8(b), small-R $\mu$ +jet	$t + \bar{t}$	$70.00 \pm 10.05$	$90.000 \pm 15.520$	$-0.50 \pm 0.05$	$34825.665 \pm 0.850$	103/16
8(c), large-R $e$ +jet	$t + \bar{t}$	$7.00 \pm 0.21$	$25.000 \pm 1.510$	$1.00 \pm 0.03$	$174997.093 \pm 1.220$	3/15
8(c), large-R $\mu$ +jet	$t + \bar{t}$	$7.00 \pm 0.20$	$24.000 \pm 1.521$	$1.00 \pm 0.03$	$174997.733 \pm 1.054$	3/15
9(a), leading, $Z_{jj}$	$t + \bar{t}$	$3.00 \pm 0.30$	$3.200 \pm 0.201$	$1.00 \pm 0.05$	$89955.257 \pm 1.523$	230/11
9(b), subleading, $Z_{jj}$	$t + \bar{t}$	$3.00 \pm 0.30$	$1.500 \pm 0.100$	$1.00 \pm 0.05$	$99992.944 \pm 1.554$	40/11
9(c), leading, pre-fit	$t + \bar{t}$	$3.00 \pm 0.11$	$4.800 \pm 0.050$	$1.00 \pm 0.02$	$93136953.879 \pm 15.400$	191/9
9(c), subleading, pre-fit	$t + \bar{t}$	$3.50 \pm 0.10$	$0.300 \pm 0.010$	$1.00 \pm 0.02$	$11991257.185 \pm 15.600$	14/6

parameter  $T$  obtained from the spectra with the lepton and dilepton channels are almost the same within the error range.

The  $p_T$  spectra of (a)(b) leading  $b$ -jets and (c)–(f) leading jets corresponding to the (a)(c)(e)  $e$ +jets channel and (b)(d)(f)  $\mu$ +jets channel in p-p collisions at (a)–

(d)  $\sqrt{s} = 7$  and (e)(f) 8 TeV are presented in Fig. 4. The symbols are cited from the experimental data measured by the ATLAS Collaboration [26, 27, 28]. The jet events were selected with  $|\eta| < 2.5$ . The curves are our fitted results with Eq. (4), in which two participant bottom quarks are considered for Figs. 4(a) and 4(b),

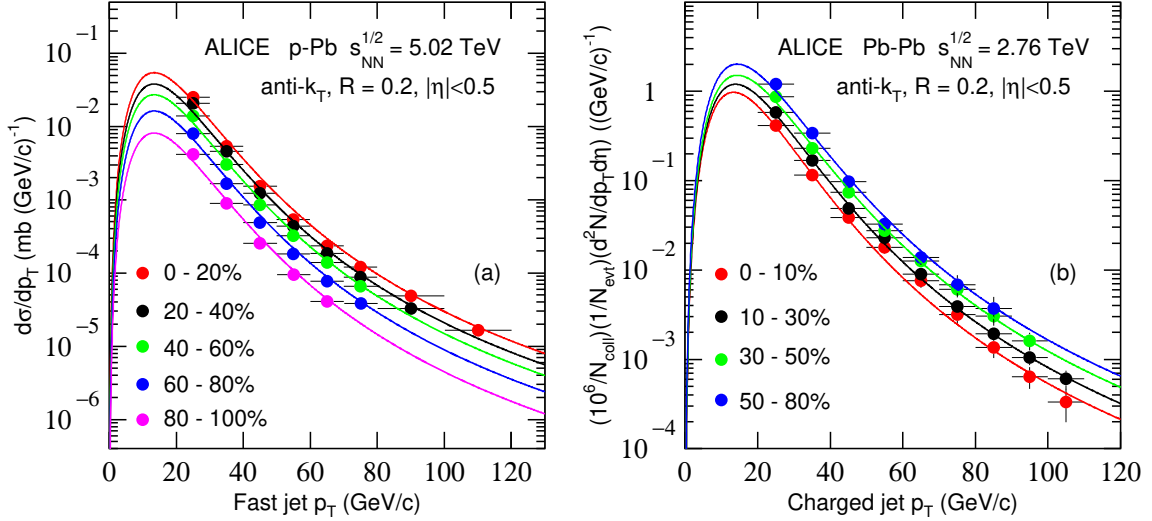


Fig. 2. Transverse momentum spectra of (a) fast jets in p-Pb collisions at  $\sqrt{s_{NN}} = 5.02$  TeV and (b) charged jets in Pb-Pb collisions at  $\sqrt{s_{NN}} = 2.76$  TeV. The different symbols are cited from the experimental data with different centrality classes measured by the ALICE Collaboration [20, 21] and the curves are our fitted results with Eq. (4).

and two participant top quarks are considered for Figs. 4(c)–4(f). The values of  $n$ ,  $T$ ,  $a_0$ ,  $N_0$ ,  $\chi^2$ , and ndof are listed in Table 1. One can see that the fold of two TP-like functions provides an approximate description on the data. The effective temperature parameter  $T$  from the  $e$ +jets channel and the  $\mu$ +jets channel are almost the same within the error range.

The reconstructed jet  $p_T$  spectra for the leading, 2<sup>nd</sup>, 3<sup>rd</sup>, 4<sup>th</sup>, and 5<sup>th</sup> order jets in the  $e$ +jets channels produced in p-p collisions at  $\sqrt{s} = 7$  TeV are shown in Fig. 5. The symbols are cited from the experimental data measured by the ATLAS Collaboration [29]. The jet events were selected with a cone radius ( $R = 0.4$ ) and wide  $\eta$  range ( $|\eta| < 2.5$ ). The curves are our fitted results with Eq. (4), in which two participant top quarks are considered. The experimental data are approximately fitted with the convolution of two TP-like functions and the values of related parameters are given in Table 1. One can see that the effective temperature parameter  $T$  decreases with the growth of jet order  $O$ .

Figure 6 presents the  $p_T$  spectra of (a) leading  $b$ -jets, (b) subleading  $b$ -jets, (c) leading jets, and (d) subleading jets produced in p-p collisions at  $\sqrt{s} = 7$  TeV. The symbols are cited from the experimental data measured by the CMS Collaboration [24, 30]. The jet events were selected with (a)(b)  $|\eta| < 2.1$  and (c)(d)  $|\eta| < 2.4$ . The curves are our fitted results with Eq. (4), in which two participant bottom quarks are considered for Figs. 6(a)

and 6(b), and two participant top quarks are considered for Fig. 6(c) and 6(d). The experimental data are approximately fitted with the convolution of two TP-like functions and the values of related parameters are given in Table 1. The values of  $T$  from the spectra of leading jets are much larger than those from the spectra of subleading jets.

Figure 7 displays the  $p_T$  spectra of (a) leading light jets, (b) subleading light jets, (c) leading jets, and (d) subleading jets produced in p-p collisions at  $\sqrt{s} = 8$  TeV, where  $N_{\text{obs}}$  denotes the number of observation. The symbols are cited from the experimental data measured by the CMS [31] and ATLAS Collaborations [32]. The jet events were selected with  $|\eta| < 2.4$ . The curves are our fitted results with Eq. (4), in which two participant charm quarks with constituent mass of 1.27  $\text{GeV}/c^2$  for each one are considered for Figs. 7(a) and 7(b), and two participant top quarks are considered for Fig. 7(c) and 7(d). The experimental data are approximately fitted with the convolution of two TP-like functions and the values of related parameters are given in Table 1. Once more, the values of  $T$  from the spectra of leading jets are much larger than those from the spectra of subleading jets.

The  $p_T$  spectra of (a)(b) small-R selected and (c)(d) large-R jets corresponding to the (a)(c)  $e$ +jets and (b)(d)  $\mu$ +jets channels produced in p-p collisions at  $\sqrt{s} = 13$  TeV are shown in Fig. 8. The symbols are

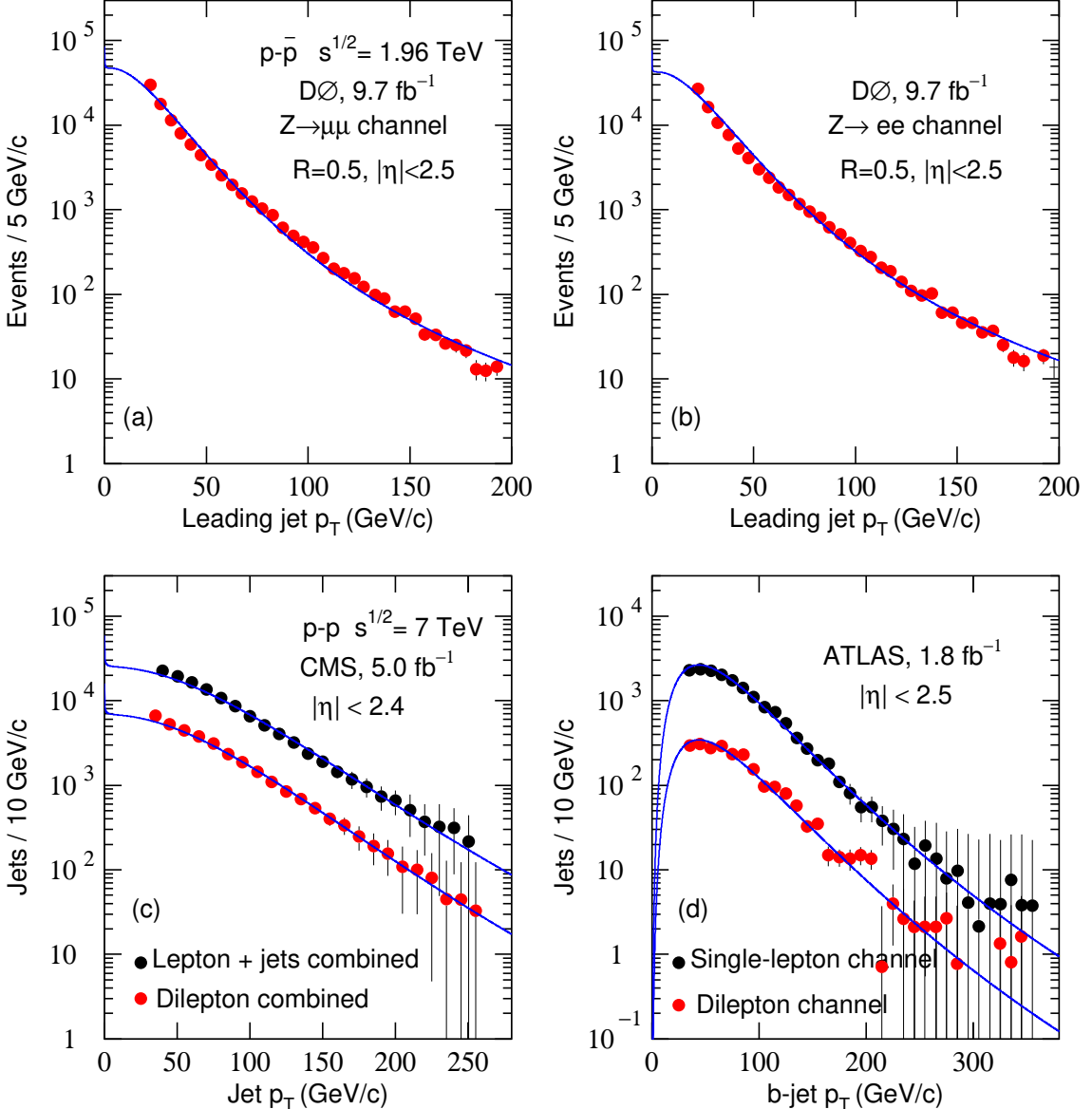


Fig. 3. Transverse momentum spectra of (a)(b) leading jets with (a)  $Z \rightarrow \mu\mu$  and (b)  $Z \rightarrow ee$  in  $p\bar{p}$  collisions at  $\sqrt{s} = 1.96$  TeV, as well as (c) jets and (d)  $b$ -jets in  $p-p$  collisions at  $\sqrt{s_{NN}} = 7$  TeV with different channels. The symbols are cited from the experimental data measured by the D0 [22, 23], CMS [24], and ATLAS Collaborations [25] and the curves are our fitted results with Eq. (4).

cited from the experimental data measured by the ATLAS Collaboration [33]. The curves are our fitted results with Eq. (4), in which two participant top quarks are considered. The experimental data are approximately fitted with the convolution of two TP-like functions and the values of related parameters are given in Table 1. One can see that the values of  $T$  from the spectra of  $e+jets$  and  $\mu+jets$  channels are almost the same within the error range.

The  $p_T$  spectra of (a) the leading jets and (b) the

subleading jets in  $Zjj$  baseline region as well as (c) the leading jets and (d) the forth jets with pre-fit produced in  $p-p$  collisions at  $\sqrt{s} = 13$  TeV are presented in Fig. 9. The symbols are cited from the experimental data measured by the ATLAS Collaboration [34, 35]. The jet events were selected with  $|y| < 2.4$  for Figs. 9(a) and 9(b), and  $|\eta| < 2.5$  for Figs. 9(c) and 9(d). The curves are our fitted results with Eq. (4), in which two participant top quarks are considered. The experimental data are approximately fitted with the convolution of

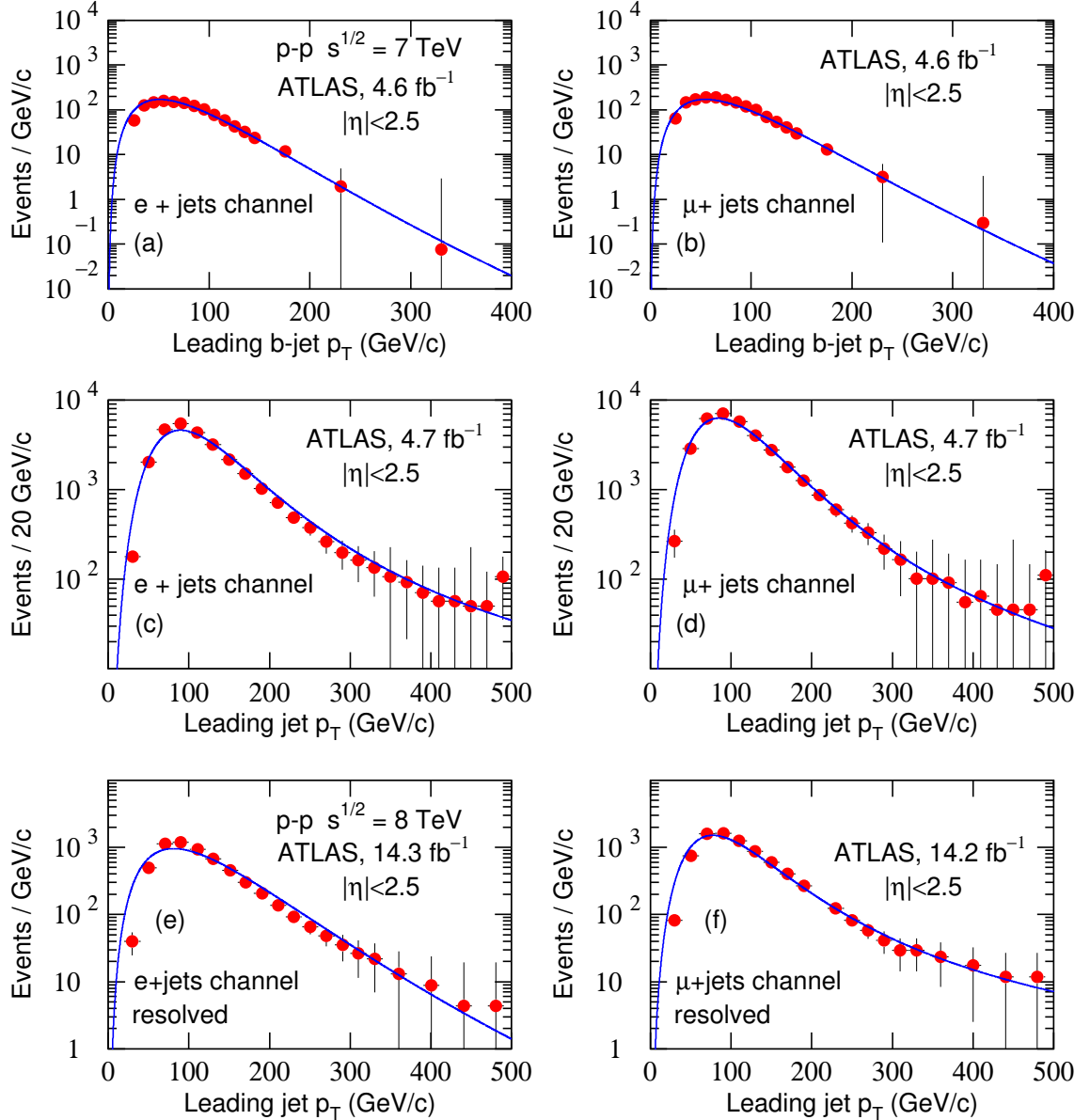


Fig. 4. Transverse momentum spectra of (a)(b) leading  $b$ -jets and (c)–(f) leading jets corresponding to the (a)(c)(e)  $e+jets$  channel and (b)(d)(f)  $\mu+jets$  channel in  $p$ - $p$  collisions at (a)–(d)  $\sqrt{s} = 7$  and (e)(f) 8 TeV. The symbols are cited from the experimental data measured by the ATLAS Collaborations [26, 27, 28] and the curves are our fitted results with Eq. (4).

two TP-like functions and the values of related parameters are given in Table 1. One can see that the values of  $T$  from the spectra of the leading jets are much larger than those from the spectra of the subleading and forth jets.

To show the trends of main parameters, Fig. 10(a) presents the relation of the effective temperature  $T$  and the centrality percentage  $C$  in  $Pb$ - $Pb$  collisions at  $\sqrt{s_{NN}} = 2.76$  TeV. The symbols represent the values of  $T$  obtained from Fig. 2 and listed in Table 1. The curve

is our fit by an exponential function

$$T = (-0.03 \pm 0.01) \exp\left(\frac{-C}{17.00 \pm 2.00}\right) + (0.15 \pm 0.01), \quad (6)$$

in which  $T$  and  $C$  are in GeV and % respectively. One can see that  $T$  increases slightly with the increase of  $C$ , or  $T$  are almost the same within the error range when  $C$  varies. The relation between  $T$  and  $C$  renders that QGP formed in central  $Pb$ - $Pb$  collisions has less influence on

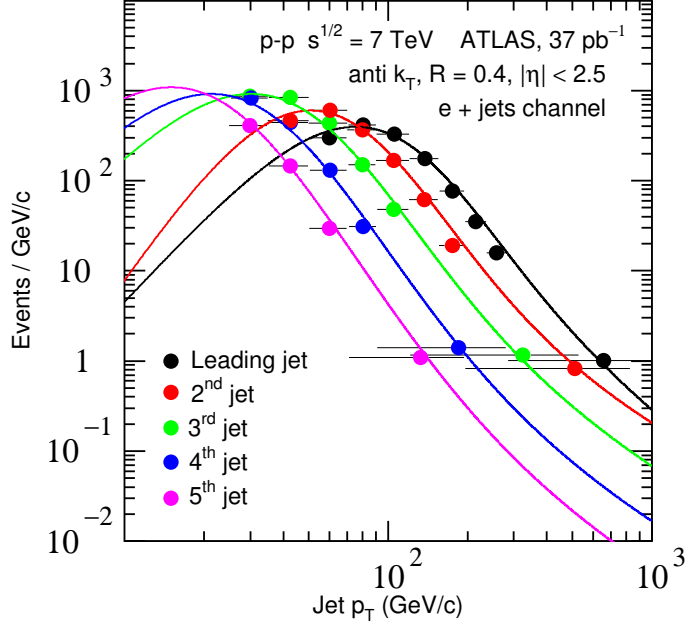


Fig. 5. Transverse momentum spectra of reconstructed jets with different orders in p-p collisions at  $\sqrt{s} = 7$  TeV. The symbols are cited from the experimental data measured by the ATLAS Collaboration [29] and the curves are our fitted results with Eq. (4).

the jet transport. Or, in the transport process of jets in QGP in central Pb-Pb collisions, jets lost less energy.

Figure 10(b) presents the relation of the effective temperature  $T$  and the jet order  $O$  in p-p collisions at  $\sqrt{s} = 7$  TeV. The symbols represent the values of  $T$  obtained from Fig. 5 and listed in Table 1. The curve is our fit by an exponential function

$$T = (11.00 \pm 0.10) \exp\left(\frac{-O}{0.80 \pm 0.01}\right) + (0.20 \pm 0.01), \quad (7)$$

in which  $T$  is in GeV. One can see that  $T$  decreases with the growth of  $O$ . This trend is natural due to the fact that the jet with high order corresponds to the source with less excitation degree.

Figure 11 shows the relations of the effective temperature  $T$  and (a) the size of interacting system, (b)  $\ell$  and di- $\ell$  channels, (c)  $\mu(\mu\mu)$  and  $e(ee)$  channels, and (d) leading and sub-leading jets. The symbols represent the values of  $T$  obtained from the above figures and listed in Table 1. One can see that  $T$  seems to not related to the system size in the error range. This is in agreement with the conclusion from Fig. 10(a) in which central collisions correspond to large system and peripheral collisions correspond to small system. In the error range,

different lepton channels show nearly the same effective temperature, which renders nearly the same excitation degree of source. At the same time, the values of  $T$  from the spectra of leading jets are much larger than those from the spectra of subleading jets, which is the same as the conclusion from Fig. 10(b).

As a parameter determining the curvature in middle- $p_T$  region and the extended range in high- $p_T$  region,  $n$  is related to the entropy index  $q$  because  $n = 1/(q-1)$ . In most cases,  $q \geq 1.2$  which is not close to 1 because  $n \leq 5$  which is not large. This implies that the source of jets does not stay at the equilibrium state. In a few cases,  $n$  is large and  $q$  is close to 1. This happens coincidentally, but not implies that the source of jets stay at the equilibrium state. This situation is different from the source of identified particles. Generally, the source of identified particles stays approximately at the equilibrium or local equilibrium state.

An a parameter determining the slope of the curve in low- $p_T$  region,  $a_0$  is elastic from negative to positive values. A negative  $a_0$  results in a cocked up distribution and a positive  $a_0$  results in a falling distribution. In many cases,  $a_0 \neq 1$  which means that it is necessary introducing  $a_0$  in the Tsallis-Pareto-type function. Due to the introduction of  $a_0$ , the revised Tsallis-Pareto-type

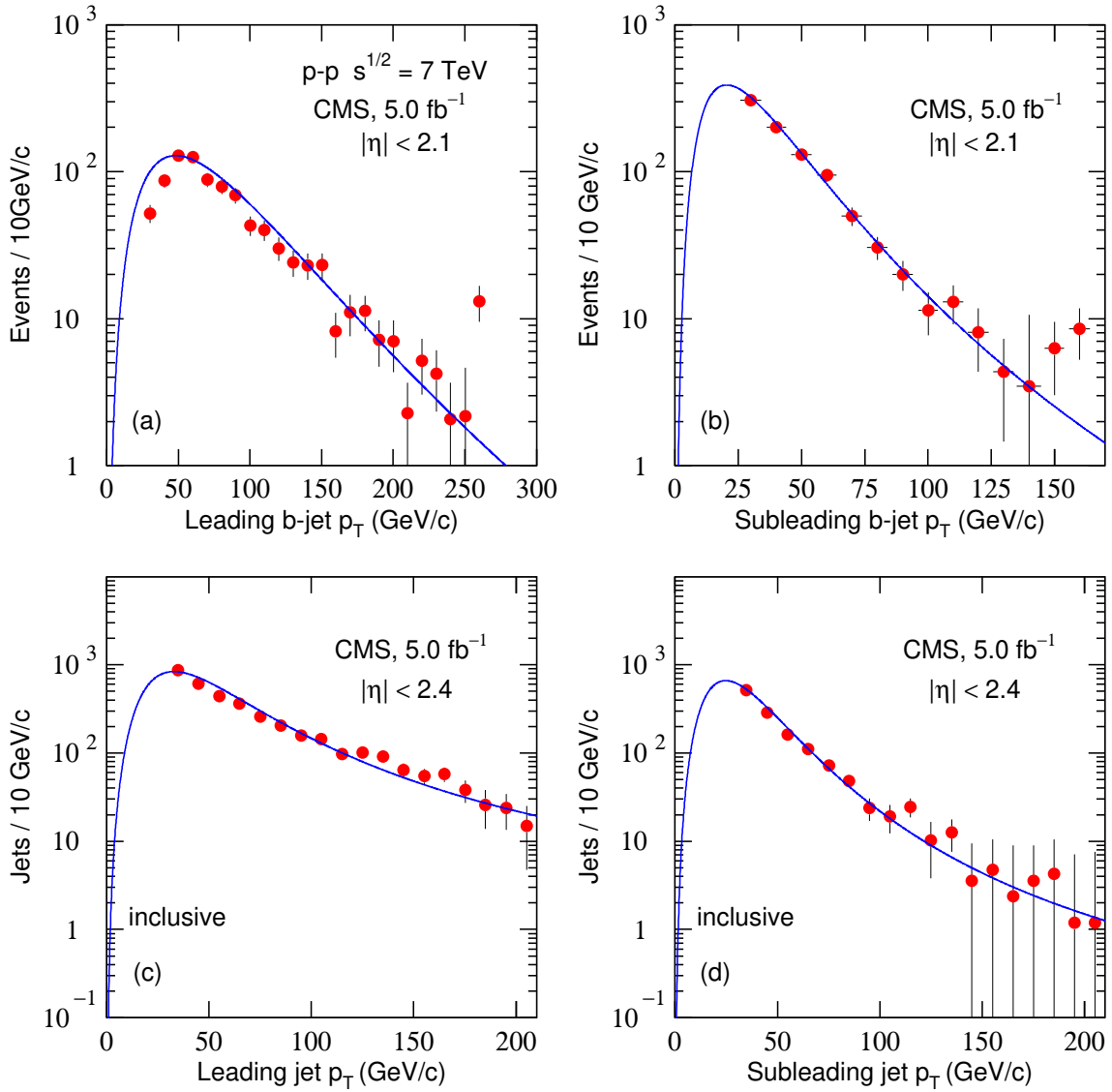


Fig. 6. Transverse momentum spectra of (a) leading  $b$ -jets, (b) subleading  $b$ -jets, (c) leading jets, and (d) subleading jets produced in  $p$ - $p$  collisions at  $\sqrt{s} = 7$  TeV. The symbols are cited from the experimental data measured by the CMS Collaboration [24, 30] and the curves are our fitted results with Eq. (4).

function, i.e. the TP-like function becomes more flexible. The convolution of two or more TP-like functions is expected to fit more  $p_T$  spectra in high energy collisions.

## 4 Summary and conclusions

We summarize here our main observations and conclusions.

(a) The transverse momentum  $p_T$  spectra of various jets selected in different conditions and produced in different collisions over an energy range from 0.2 to 13 TeV are fitted by the convolution of two TP-like func-

tions, where the TP-like function is a revised Tsallis–Pareto-type function. The experimental data recorded by various collaborations are approximately fitted by the mentioned convolution.

(b) From the fit on the  $p_T$  spectra of charged jets produced in Pb-Pb collisions at  $\sqrt{s} = 2.76$  TeV with different centrality intervals, we know that the effective temperature  $T$  increases slightly with increasing the centrality percentage, or  $T$  is almost the same in the error range when the centrality changes. Meanwhile,  $T$  from the spectra of jets in  $p$ - $p$ , d-Au, and Au-Au collisions at 0.2 TeV does not show the size dependence. This is

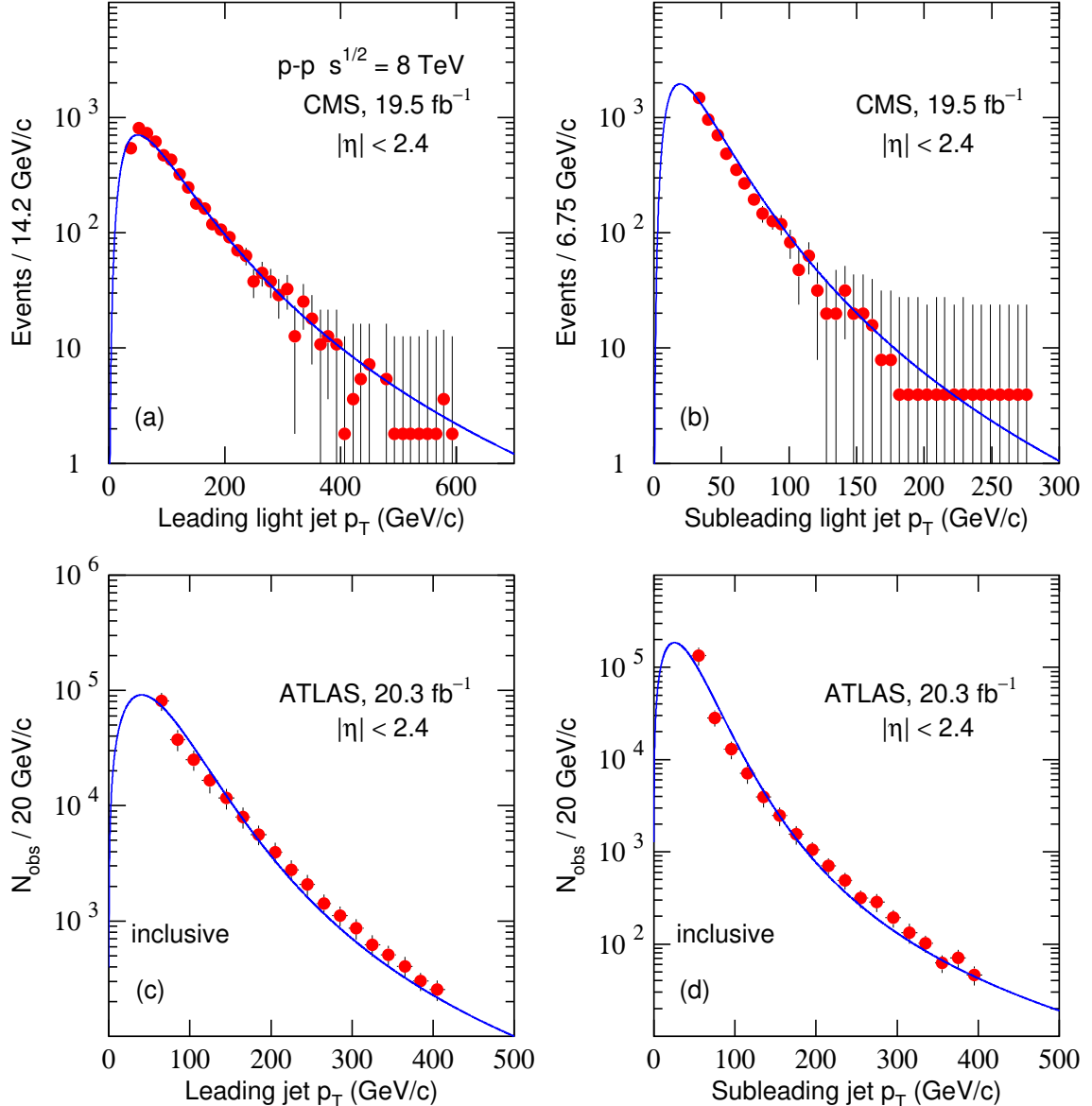


Fig. 7. Transverse momentum spectra of (a) leading light jets, (b) subleading light jets, (c) leading jets, and (d) subleading jets produced in p-p collisions at  $\sqrt{s} = 8 \text{ TeV}$ . The symbols are cited from the experimental data measured by the CMS [31] and ATLAS Collaborations [32] and the curves are our fitted results with Eq. (4).

consistent to the nearly independence of  $T$  on centrality.

(c) The values of  $T$  from the spectra of leading jets are much larger than those from the spectra of subleading jets due to the leading jets undergone more violent scattering. As expected,  $T$  extracted from the reconstructed jets produced in p-p collisions at  $\sqrt{s} = 7 \text{ TeV}$  decreases with the growth of the jet order. In addition,  $T$  from the lepton and dilepton channels are almost the same, which means that these jets have common property.

(d) The parameter  $n$  determines the curvature in

middle- $p_T$  region and the extended range in high- $p_T$  region. Meanwhile,  $n$  is related to the entropy index  $q$  because  $n = 1/(q - 1)$ . Generally,  $n$  is not too large. This means that  $q$  is not close to 1 and the source of jets does not stay at the equilibrium state. This is different from the source of identified particles which stays approximately at the equilibrium or local equilibrium state.

(e) The parameter  $a_0$  determines the slope of the curve in low- $p_T$  region. A negative  $a_0$  results in a cocked up distribution and a positive  $a_0$  results in a

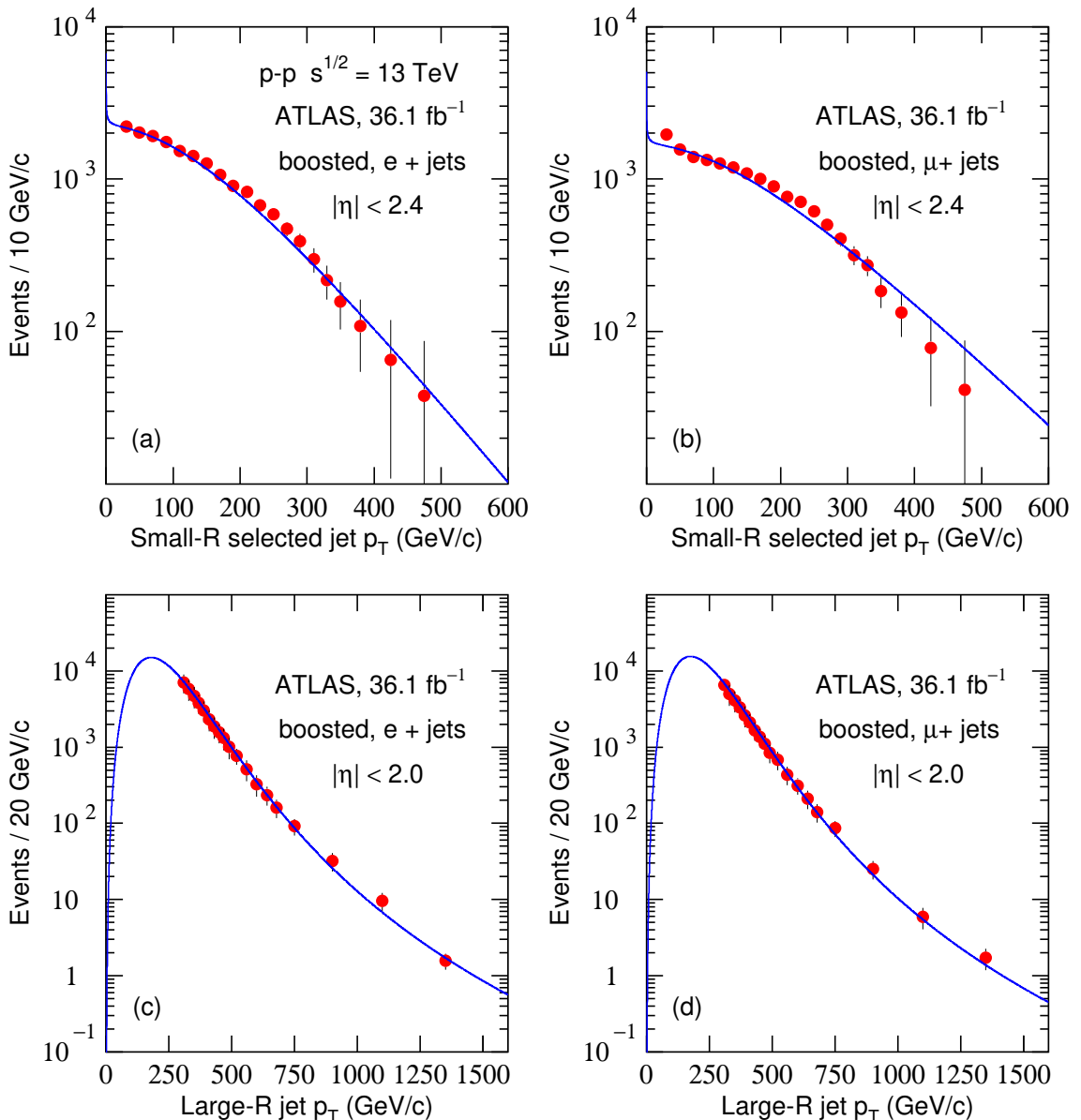


Fig. 8. Transverse momentum spectra of (a)(b) small-R selected and (c)(d) large-R jets corresponding to the (a)(c)  $e+jets$  and (b)(d)  $\mu+jets$  channels produced in  $p\text{-}p$  collisions at  $\sqrt{s} = 13$  TeV. The symbols are cited from the experimental data measured by the ATLAS Collaboration [33] and the curves are our fitted results with Eq. (4).

falling distribution. Due to the introduction of  $a_0$  in the Tsallis–Pareto-type function, the revised function, i.e. the TP-like function, becomes more flexible. The convolution of two or more TP-like functions is expected to have more applications.

#### Data Availability

The data used to support the findings of this study are included within the article and are cited at relevant places within the text as references.

#### Ethical Approval

The authors declare that they are in compliance with ethical standards regarding the content of this paper.

#### Disclosure

The funding agencies have no role in the design of the study; in the collection, analysis, or interpretation of the data; in the writing of the manuscript; or in the decision to publish the results.

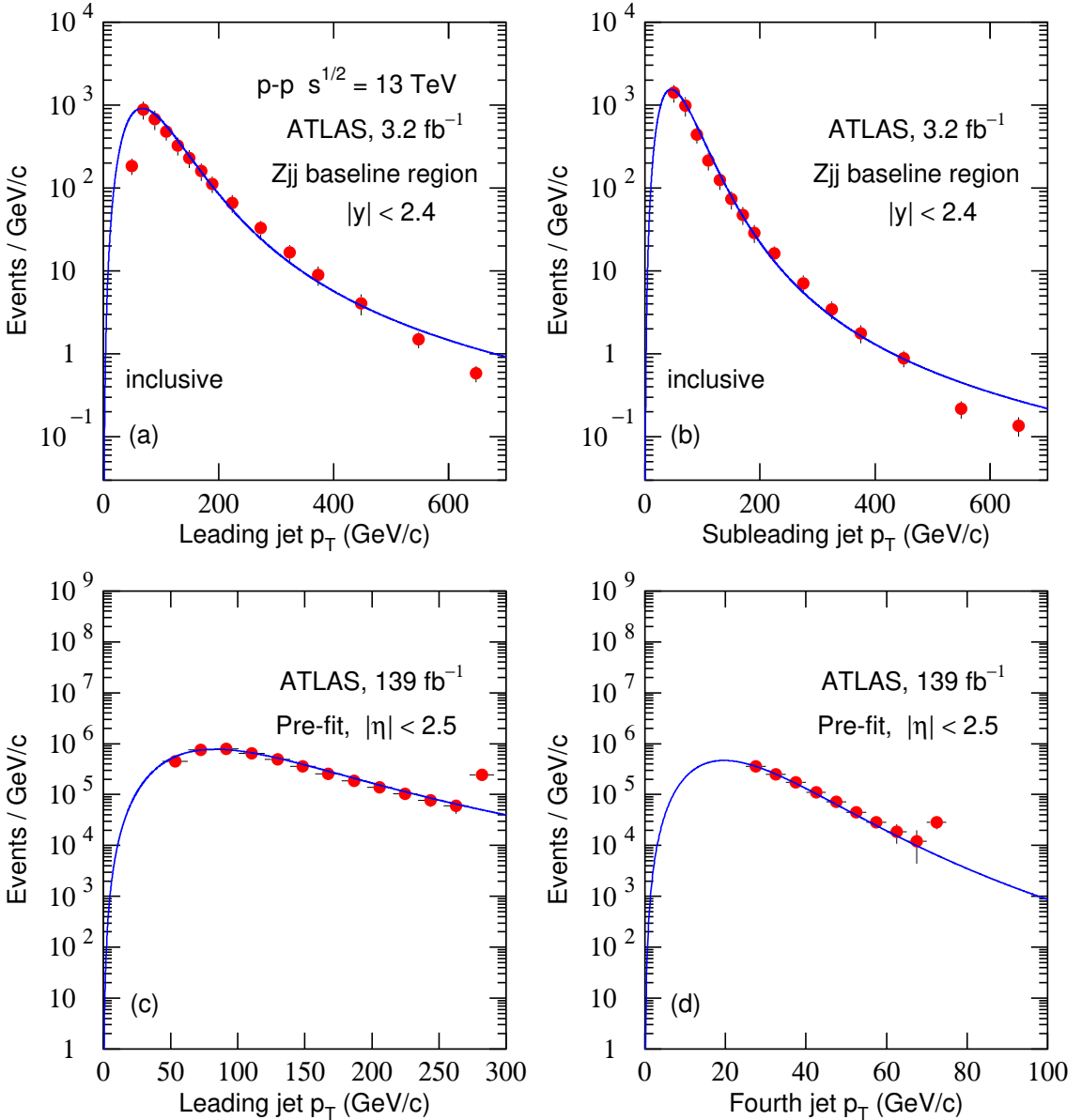


Fig. 9. Transverse momentum spectra of (a) the leading jets and (b) the subleading jets in  $Z_{jj}$  baseline region as well as (c) the leading jets and (d) the forth jets with pre-fit produced in p-p collisions at  $\sqrt{s} = 13$  TeV. The symbols are cited from the experimental data measured by the ATLAS Collaboration [34, 35] and the curves are our fitted results with Eq. (4).

### Conflict of Interest

The authors declare that there are no conflicts of interest regarding the publication of this paper.

### Acknowledgments

The work of the first author (Y.M.T.) was supported by Shanxi University. The work of the second author (P.P.Y.) was supported by the China Scholarship Council (Chinese Government Scholarship) under Grant No.

202008140170 and the Shanxi Provincial Innovative Foundation for Graduate Education under Grant No. 2019SY053. The work of the third author (F.H.L.) was supported by the National Natural Science Foundation of China under Grant Nos. 11575103 and 11947418, the Scientific and Technological Innovation Programs of Higher Education Institutions in Shanxi (STIP) under Grant No. 201802017, the Shanxi Provincial Natural Science Foundation under Grant No. 201901D111043, and the Fund for Shanxi “1331 Project” Key Subjects Construction.

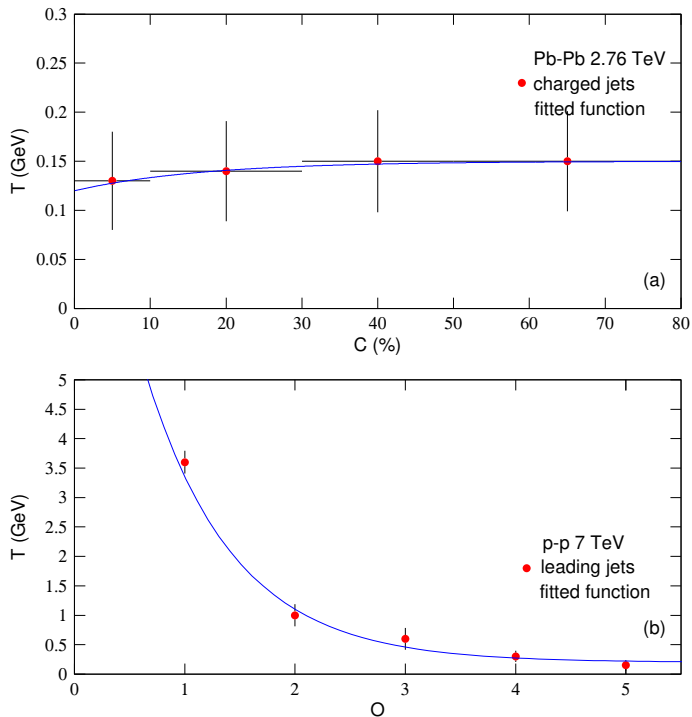


Fig. 10. The relations of (a) the effective temperature parameter  $T$  and the centrality percentage  $C$  in Pb-Pb collisions at  $\sqrt{s} = 2.76$  TeV, as well as (b)  $T$  and the jet order  $O$  in p-p collisions at  $\sqrt{s} = 7$  TeV. The symbols represent the values of  $T$  obtained from Figs. 2 and 5 and listed in Table 1. The curves are our fitted results with Eqs. (6) and (7) respectively.

## References

- [1] J. Adams et al. (STAR Collaboration), “Experimental and theoretical challenges in the search for the quark-gluon plasma: The STAR Collaboration’s critical assessment of the evidence from RHIC collisions,” *Nuclear Physics A*, **757**, pp. 102–183, 2005.
- [2] K. Adcox et al. (PHENIX Collaboration), “Formation of dense partonic matter in relativistic nucleus–nucleus collisions at RHIC: Experimental evaluation by the PHENIX Collaboration,” *Nuclear Physics A*, **757**, pp. 184–283, 2005.
- [3] J. F. Grosse-Oetringhaus for the ALICE Collaboration, “Overview of ALICE results at Quark Matter 2014,” *Nuclear Physics A*, **931**, pp. 22–31, 2014.
- [4] T. Mizoguchi, M. Biyajima, N. Suzuki, “Analyses of whole transverse momentum distributions in  $p\bar{p}$  and  $pp$  collisions by using a modified version of Hagedorn’s formula,” *International Journal of Modern Physics A*, vol. 32, article 1750057, 2017.
- [5] F.-H. Liu, Y.-Q. Gao, T. Tian, and B.-C. Li, “Unified description of transverse momentum spectrums contributed by soft and hard processes in high-energy nu-

clear collisions," *The European Physical Journal A*, vol. 50, article 94, 2014.

- [6] R. Hagedorn, “Multiplicities,  $p_T$  distributions and the expected hadron  $\rightarrow$  quark-gluon phase transition,” *La Rivista del Nuovo Cimento*, vol. 6, no. 10, pp. 1–50, 1983.
- [7] E. K. G. Sarkisyan and A. S. Sakharov, “Multihadron production features in different reactions,” *AIP Conference Proceedings*, vol. 828, pp. 35–41, 2006.
- [8] E. K. G. Sarkisyan and A. S. Sakharov, “Relating multihadron production in hadronic and nuclear collisions,” *The European Physical Journal C*, vol. 70, pp. 533–541, 2010.
- [9] A. N. Mishra, R. Sahoo, E. K. G. Sarkisyan, and A. S. Sakharov, “Effective-energy budget in multiparticle production in nuclear collisions,” *The European Physical Journal C*, vol. 74, article 3147, 2014.
- [10] E. K. G. Sarkisyan, A. N. Mishra, R. Sahoo, and A. S. Sakharov, “Multihadron production dynamics exploring the energy balance in hadronic and nuclear collisions,” *Physical Review D*, vol. 93, article 054046, 2016.
- [11] E. K. G. Sarkisyan, A. N. Mishra, R. Sahoo, and A. S. Sakharov, “Centrality dependence of midrapidity density from GeV to TeV heavy-ion collisions in the effective-energy universality picture of hadroproduction,” *Physical Review D*, vol. 96, article 054027, 2017.

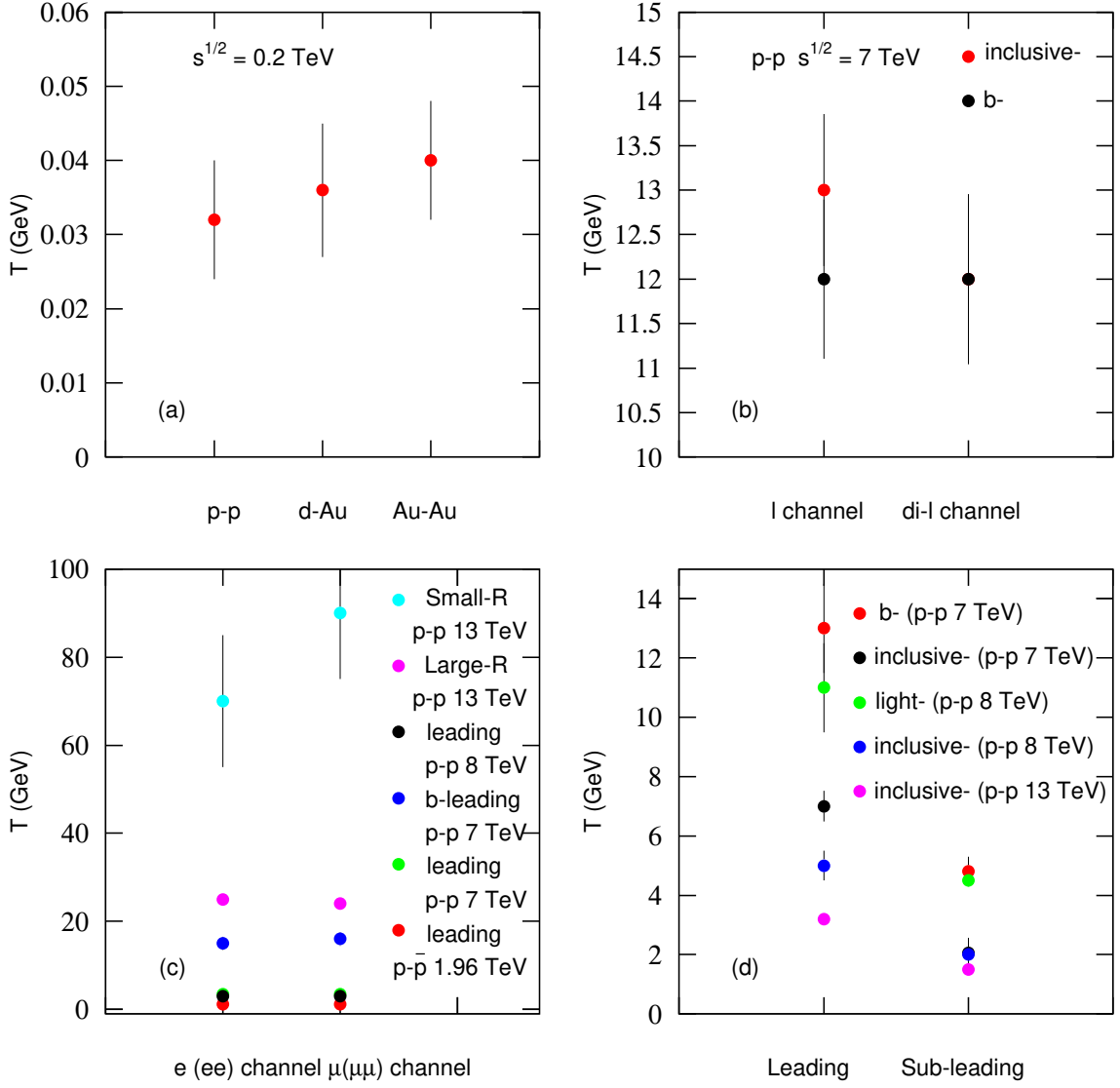


Fig. 11. The relations of the effective temperature parameter  $T$  and (a) the size of interacting system, (b) the  $\ell$  and di- $\ell$  channels, (c) the  $e$  ( $ee$ ) and  $\mu$  ( $\mu\mu$ ) channels, as well as (d) the leading and sub-leading jets. The symbols represent the values of  $T$  obtained from various figures and listed in Table 1.

tion,” *Physical Review D*, vol. 94, article 011501(R), 2016.

[12] E. K. G. Sarkisyan, A. N. Mishra, R. Sahoo, and A. S. Sakharov, “Effective-energy universality approach describing total multiplicity centrality dependence in heavy-ion collisions,” *EPL*, vol. 127, article 62001, 2019.

[13] A. N. Mishra, A. Ortiz, and G. Paić, “Intriguing similarities of high- $p_T$  particle production between  $pp$  and  $A$ - $A$  collisions,” *Physical Review C*, vol. 99, article 034911, 2019.

[14] S. Chatrchyan et al. (CMS Collaboration), “Study of the inclusive production of charged pions, kaons, and protons in pp collisions at  $\sqrt{s} = 0.9$ , 2.76, and 7 TeV,” *The European Physical Journal C*, vol. 72, article 2164, 2012.

[15] P.-P. Yang, F.-H. Liu, R. Sahoo, “A new description of transverse momentum spectra of identified particles produced in proton-proton collisions at high energies,” *Advances in High Energy Physics*, vol. 2020, article 6742578, accepted, 2020. arXiv:1909.13235 [hep-ph], 2019.

[16] L. Adamczyk et al. (STAR Collaboration), “Jet-hadron correlations in  $\sqrt{s_{NN}} = 200$  GeV p+p and central Au+Au collisions,” *Physics Review Letters*, vol. 112, article 122301, 2014.

[17] J. Kapitán for the STAR Collaboration, “Jets in 200

GeV p+p and d+Au collisions from the STAR experiment at RHIC,” *Journal of Physics: Conference Series*, vol. 270, article 012015, 2011.

[18] J. Adam et al. (STAR Collaboration), “Longitudinal double-spin asymmetries for dijet production at intermediate pseudorapidity in polarized pp collisions at  $\sqrt{s} = 200$  GeV,” *Physics Review D*, vol. 98, article 032011, 2018.

[19] M. Cacciari, G. P. Salam, G. Soyez, “The anti- $k_t$  jet clustering algorithm,” *Journal of High Energy Physics*, vol. 2008, no. 4, article 63, 2008.

[20] J. Adam et al. (ALICE Collaboration), “Centrality dependence of charged jet production in p-Pb collisions at  $\sqrt{s_{NN}} = 5.02$  TeV,” *The European Physical Journal C*, vol. 76, article 271, 2016.

[21] B. Abelev et al. (ALICE Collaboration), “Measurement of charged jet suppression in Pb-Pb collisions at  $\sqrt{s_{NN}} = 2.76$  TeV,” *Journal of High Energy Physics*, vol. 2014, no. 3, article 13, 2014.

[22] V. M. Abazov et al. (D0 Collaboration), “Measurement of the ratio of differential cross sections  $\sigma(p\bar{p} \rightarrow Z + \text{bjet})/\sigma(p\bar{p} \rightarrow Z + \text{jet})$  in  $p\bar{p}$  collisions at  $\sqrt{s} = 1.96$  TeV,” *Physics Review D*, vol. 87, article 092010, 2013.

[23] V. M. Abazov et al. (D0 Collaboration), “Studies of  $W$  boson plus jets production in  $p\bar{p}$  collisions at  $\sqrt{s} = 1.96$  TeV,” *Physics Review D*, vol. 88, article 092001, 2013.

[24] S. Chatrchyan et al. (CMS Collaboration), “Measurement of jet multiplicity distributions in  $t\bar{t}$  production in pp collisions at  $\sqrt{s} = 7$  TeV,” *The European Physical Journal C*, vol. 74, article 3014, 2014.

[25] G. Aad et al. (ATLAS Collaboration), “Measurement of jet shapes in top-quark pair events at  $\sqrt{s} = 7$  TeV using the ATLAS detector,” *The European Physical Journal C*, vol. 73, article 2676, 2013.

[26] G. Aad et al. (ATLAS Collaboration), “Measurements of normalized differential cross sections for  $t\bar{t}$  production in pp collisions at  $\sqrt{s} = 7$  TeV using the ATLAS detector,” *Physics Review D*, vol. 90, article 072004, 2014.

[27] G. Aad et al. (ATLAS Collaboration), “Search for  $t\bar{t}$  resonances in the lepton plus jets final state with ATLAS using  $4.7 \text{ fb}^{-1}$  of pp collisions at  $\sqrt{s} = 7$  TeV,” *Physics Review D*, vol. 88, article 012004, 2013.

[28] D. Benjamin for the ATLAS Collaboration, “A search for  $t\bar{t}$  resonances in the lepton plus jets final state with ATLAS using  $14 \text{ fb}^{-1}$  of pp collisions at  $\sqrt{s} = 8$  TeV,” *EPJ Web of Conferences*, vol. 60, article 20044, 2013.

[29] G. Aad et al. (ATLAS Collaboration), “Measurement of the  $t\bar{t}$  production cross-section as a function of jet multiplicity and jet transverse momentum in 7 TeV proton-proton collisions with the ATLAS detector,” *Journal of High Energy Physics*, vol. 2015, no. 1, article 20, 2015.

[30] S. Chatrchyan et al. (CMS Collaboration), “Measurement of the production cross sections for a Z boson and one or more b jets in pp collisions at  $\sqrt{s} = 7$  TeV,” *Journal of High Energy Physics*, vol. 2014, no. 6, article 120, 2014.

[31] CMS Collaboration, “Search for pair production of resonances decaying to a top quark plus a jet in final states with two leptons,” CERN Document Server – CMS Physics Analysis Summaries: CMS-PAS-B2G-12-008, 2012, <https://cds.cern.ch/record/1630845/>

[32] G. Aad et al. (ATLAS Collaboration), “Measurement of the electroweak production of dijets in association with a Z-boson and distributions sensitive to vector boson fusion in proton-proton collisions at  $\sqrt{s} = 8$  TeV using the ATLAS detector,” *Journal of High Energy Physics*, vol. 2014, no. 4, article 31, 2014.

[33] M. Aaboud et al. (ATLAS Collaboration), ‘Search for heavy particles decaying into top-quark pairs using lepton-plus-jets events in proton-proton collisions at  $\sqrt{s} = 13$  TeV with the ATLAS detector,” *The European Physical Journal C*, vol. 78, article 565, 2018.

[34] M. Aaboud et al. (ATLAS Collaboration), “Measurement of the cross-section for electroweak production of dijets in association with a Z boson in pp collisions at  $\sqrt{s} = 13$  TeV with the ATLAS detector,” *Physics Letters B*, vol. 775, pp. 206–228, 2017.

[35] ATLAS Collaboration, “Measurement of the  $t\bar{t}$  production cross-section in the lepton+jets channel at  $\sqrt{s} = 13$  TeV with the ATLAS experiment,” CERN Document Server – ATLAS Note: ATLAS-CONF-2019-044, 2019, <https://cds.cern.ch/record/2690717/>